COMPUTER-AIDED DESIGN & APPLICATIONS, 2016
VOL. 13, NO. 3, 295–308
http://dx.doi.org/10.1080/16864360.2015.1114387

# Shrinkwrap geometry defeaturing for finite element analysis for a wheel and hub model

Matthew G. Pike[1], David X. Feng[2] and Michael R. Myers[1]

[1]Vanderbilt University; [2]School for Science and Math at Vanderbilt

**ABSTRACT**

This manuscript presents an automated approach to accurately estimate structural performance for component assemblies using a shrinkwrap geometry defeaturing process for a wheel and hub model. Defeaturing is a popular geometry simplification technique that suppresses features within the geometry to decrease computational resources and time. Shrinkwrap defeaturing is an automated modeling technique that represents the exterior shape of the original full-featured geometry with a collection of surfaces for an abstract representation. The shrinkwrap defeaturing can be used on full-featured computer aided design components that are parts of an assembly but are not undergoing structural analysis and are included to transmit loads within the assembly. Of interest is the automated finite element structural analysis of the assembly. The proposed shrinkwrap approach is reviewed and assessed with a full-featured geometry model as well as other geometry defeaturing methods. A numerical example of a wheel and hub is presented to show that the proposed shrinkwrap approach displays better estimated structural performance than use of spider modeling, which incorporates 1D-3D model connections.

**KEYWORDS**

Abstract geometry; FEA; defeatured geometry; shrinkwrap; structural analysis

## 1. Introduction

Finite element analysis (FEA) has become a common technique for the review of structural systems. Structures with complex geometry and loads can be difficult to analyze using basic techniques. With the use of FEA, complex structures are conveniently analyzed. The convenience of commercial FEA programs has significantly aided the analysis of complex structures by removing the need to develop the governing equations and the mathematics in the model. The user is able to define the geometry, loads and boundary conditions and predict the structural performance of the system. A review of FEA can be found in [44].

Commercialized FEA products have paved the way for analysis of intricate and sophisticated models, but errors still arise. For models with complex geometry, stress singularities (infinite stress at a point) can arise in the analysis due to various reasons, including the mesh of the model. Work on estimating singularities in finite elements and how to address them have been developed [32], [42], [24]. Common occurrences that develop singularities include cracks and crack growth [53], [41] and the mesh dependence on them [43]. Methods proposed to overcome the presence of singularities include computing stress singularities at bimaterial interfaces [45], discretizing finite elements to avoid singularities [48], [8] and an alternating procedure for solving singularity problems [23].

Complex geometry can also lead to singularities that may produce irregular results as well as increase computational time due to the high-resolution mesh that the geometry requires. Model simplification can overcome various geometry complexities. The popular geometry simplification technique of defeaturing, which suppresses features within the computer-aided design (CAD) geometry, can alleviate the issue of singularities and decrease computational time. Defeaturing of geometry typically removes geometric details, such as holes, sharp corners and indents to create smooth surfaces [52]. This geometric defeaturing can significantly reduce the complexity of the model and the computational effort of mesh generation in finite element modeling. Defeaturing is also utilized when the specific geometric details are not needed for analysis [13] and when only the general representation of the geometry is needed to transfer load [12].

When CAD geometry is imported into computer-aided engineering (CAE) systems, the integration of the

**CONTACT** Matthew G. Pike Matthew.G.Pike@vanderbilt.edu

geometry may not have the same exact representation as the original [18]. The mesh generation changes the shape of models [3], [27], [6], [38] and ultimately produces errors in model estimation [7], [19]. Theories to estimate errors in modified geometry include using a dual weighted residual method [22], and other methods [51], [21], [20]. To minimize error in analysis, methods to defeature geometry include mesh constraint topology for finite elements [11], removing features below a threshold value [34] and mesh optimization with error of geometry simplification [2]. A review of simplification techniques has been compiled [48].

Geometry defeaturing of models has seen development using spider modeling, which represents featured geometry with rigid 1D beam elements in a web-like fashion [1],[47]. The beam elements are able to transfer the load to other components. Since featured geometry is replaced and represented by only a few elements, as compared to numerous elements in a full-featured model, the computation time decreases significantly. Use of spider modeling to represent bolted joints [16], [28] and rotors [54] has been documented. Recent work with crack tips has used spider modeling to define and analyze the crack tips in a domain [5]. Although spider models can reduce computational time, errors with the process are prevalent. The 1D beam elements connect to the 3D model, which can result in spurious stress concentrations in the model [26]. The connection of the spider elements to the finite element mesh must be properly placed and constructed to transfer load. Criteria for connection of the beam elements using a minimum of eight nodes on the featured model have been proposed [31].

Geometry defeaturing is especially useful when analyzing assemblies. Small automotive assemblies, such as hub and axle models [50], [40], [55], [30], wheel bearings [29], clutch models [33] and rail wheel models [35], display the process of assembly analysis. Defeaturing can be easily done for various components in these small assemblies. Considering larger models, such as the entire automobile, the process of defeaturing becomes a challenge. For instance, the defeaturing process for spider modeling is typically done manually, due to the sensitivity of spider element placement and connection to finite element nodes. This manual process becomes burdensome when analyzing large assemblies.

The process of automated FEA design has been incorporated to efficiently analyze various models [10], [4], [37], [35], [17]. The automated process in large model assemblies provides significant reduction in computational time in mesh creation analysis and adaptive remeshing. The incorporation of automated defeaturing has been introduced [46], [9] for the mesh generation process in FEA, which leads to decreased computational time in both the meshing process and analysis due to the size of the model.

In this manuscript, we present an approach to accurately estimate the structural performance for component design of a wheel and hub model using shrinkwrap defeaturing of geometry in an automated FEA process. Shrinkwrap defeaturing is an automated modeling technique that represents the exterior shape of the original full-featured geometry with a collection of surfaces for an abstract representation. In this work, shrinkwrap defeaturing is performed in PTC® Creo Parametric 2.0 and is utilized in an in-house, open-source, automated process. The proposed approach handles arbitrary 3D CAD component models for the structural analysis of the CAD geometry for given loading and boundary conditions. We compare the geometry defeaturing approaches of manual simplified geometry, spider modeling and shrinkwrap modeling. The proposed shrinkwrap approach is assessed with an example component model for full-featured geometry to evaluate the structural performance.

The remainder of this manuscript is arranged as follows. Section 2 provides an overview of the tool suite used to model and structurally analyze CAD geometry. Section 3 reviews full-featured geometry modeling. Manual simplified geometry is addressed in Section 4. Defeatured geometry in the form of spider modeling is summarized in Section 5. Section 6 discusses shrinkwrapped, defeatured geometry. Section 7 explains the method and problem formulation for the geometry studied in this manuscript. Analysis results are presented in Section 8. Conclusions and future research directions in this area are discussed in Section 9.

## 2. Meta tool suite

In this manuscript, we seek to evaluate the structural performance of defeatured geometry models with reference to a full-featured geometry model. We employ an in-house developed, open-source code for the automated analysis.

The in-house code is part of the META tool suite, which is an open-source tool set that implements the development of a portfolio of programs to address the revolutionary approaches for designing, verifying, and manufacturing complex systems [15] The tool suite is able to significantly decrease prototype development time, provide accurate analysis, adapt to various models and able to estimate build cost and lead-time. The core concepts of the META tool suite include the availability of multi-phenomenon components and component model libraries, automated system and analysis composition, model abstraction, design verification and complexity

driven design. The META tool suite is capable of handling a variety of systems such as physical design, CAD assembly, FEA, computational fluid dynamics (CFD), blast, ballistics and reliability, among many others. The META tool suite integrates various commercial and open-source programs, including CAD modeling with PTC® Creo Parametric 2.0 and finite element modeling with Dassault Systèmes Abaqus, used in this work.

CAD and FEA modeling are utilized from the META tool suite in this work to investigate structural performance. An automated process used to incorporate the preprocessing, mesh generation, solver and analysis of the results. The automated process handles 3D models consisting of various components for a variety of shapes, materials, loadings, boundary conditions and connections. The components are assembled together automatically, creating a model assembly for analysis. Each component is analyzed to understand the behavior from the component interactions. The automated process is set up to handle defeaturing of original CAD geometry using the proposed shrinkwrap approach. Geometric defeaturing can lead to geometry overlap in the assembly. The tool suite overcomes this obstacle by automatically modifying the defeatured component to fit to the featured geometry of adjacent components. The methods in this work could also be performed manually, but the tool suite is used to take advantage of the automated feature and to demonstrate the tool suite capabilities.

This work presents an example of a wheel and hub assembly to demonstrate the proposed approach. The wheel and hub are a sub assembly from a forklift model assembly [14] as shown in Fig. 1. The forklift dimensions are approximately 2.7 m in length, 2.2 m in height and 1.1 m wide. The mass of the forklift is approximately 3 metric tons. Although the META tool suite supports adaptive re-meshing in FEA modeling, adaptive re-meshing is not used for this work.

## 3. Full-featured geometry

For the remainder of this manuscript, we consider a three-component wheel and hub model displayed in Fig. 2. The hub is modeled with an outside diameter of 178 mm and a thickness of 12.7 mm. The inner diameter of the hub (where an axle is typically located) is 57 mm. There are eight 12.7 mm diameter holes for bolt connections located between the inside and outside diameters of the hub. The wheel has a diameter of 305 mm, width of 175 mm and web thickness of 6.35 mm. The web of the wheel contains eight holes for bolt connections and a 76 mm diameter hole in the center of the web (similar to the hub for the typical axle location). The base of the adapter is 175 mm by 200 mm and is created such that the wheel surface is flush with the adapter. The wheel and hub components are taken from the forklift model described in the previous section. An adapter component, which is attached to the bottom of the wheel, conforms to the geometry of the wheel and is included in this model so that a vertical load can be applied without introducing a singularity in the wheel.

In this section, the full-featured geometry of all components is considered (Fig. 2) for the analysis. We are interested in the structural integrity of the hub in this

**Figure 1.** Featured forklift CAD geometry. Forklift is approximately 2.7 m in length, 2.2 m in height and 1.1 m wide with a mass of 3 metric tons [13].

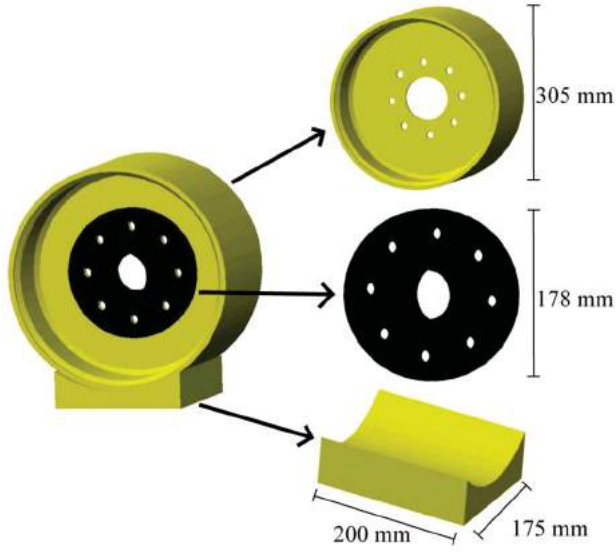


**Figure 2.** CAD model of featured wheel and hub geometry. Adapter component at the bottom of the wheel is incorporated for vertical load transfer. Each component is displayed individually to fully show the geometry.

work because we assume that we manufacture the hub component, but utilize a "bought" wheel component that has already been structurally analyzed for the prescribed loading. The hub contains eight boltholes around the center shaft of the hub. Bolts are not considered in this work. The hub is connected to the wheel (via the bolts in reality) on the inside face of the wheel web. The contact surfaces of the hub and wheel are considered bonded to replace the bolted joint. The wheel has hole openings for the boltholes and the inside diameter of the hub. The full-featured geometry model utilizes the automated system in the tool suite.

## 4. Manual simplified geometry

In structural analysis in this work, we are concerned with the behavior of the hub. Therefore, we keep the same CAD geometry of the full-featured hub and defeature other components to gain an accurate representation in the structural analysis while reducing computational time. Typical reasons to defeature geometry include: geometry that is too detailed or complex, geometry that is insignificant in the model, not enough detail in the geometry and geometry that doesn't exactly match the physical component (e.g., a proprietary component might have an associated CAD model that isn't complete). For the purpose of this work, we utilize defeatured geometry because we are only interested in the analysis of one component in the assembly and need to represent the remaining geometry to transfer the load between components.

We look to defeature the geometry of the wheel in this work. The adapter component attached to bottom of the wheel is automatically modified to fit the geometry of the wheel. The full-featured geometry of the wheel include numerous holes and sharp edges that can lead to increased computational time with mesh generation and solving of the finite element model as well as possible development of singularities due to the detailed geometry.

The simplest form of geometry defeaturing for the wheel is to enclose all of the holes in the web. Removing the holes in the web creates a smoother surface and requires fewer finite elements, resulting in faster analysis. A geometric representation of the manual defeatured wheel and hub model is displayed in Fig. 3. The enclosure of the holes in the web of the wheel is performed manually by altering the geometry in the CAD software. Modifying the wheel in this preprocessing step leads to the use of the automated process for the structural analysis of the manual simplified geometry wheel and hub model.

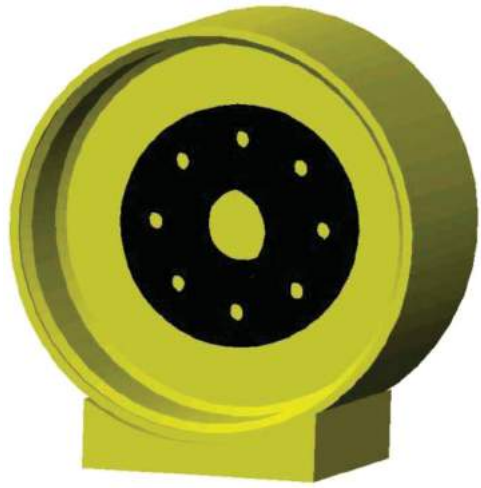

**Figure 3.** CAD model of wheel and hub with manual simplified geometry of the wheel. The wheel is defeatured by enclosing all of the holes in the web. Adapter component at the bottom of the wheel is incorporated for vertical load transfer.

## 5. Spider geometry modeling

Spider modeling is a method used to represent the transfer of load between components in assemblies without representing the full-featured geometry of a particular component within the assembly. Spider modeling takes featured geometry and represents it using rigid 1D beam elements in a web-like fashion (e.g., [16]). The rigid elements are typically of the same length and ordered in a circular web around a center point. The rigid elements connect to other (3D full-featured) geometry to transfer load between the different components. With the spider model, the new modified geometry is represented using a few elements, resulting in minimal computational time. Spider modeling has been shown to decrease the computation time, but include errors in the analysis [47]. Therefore, to minimize the error, we must determine how many spider elements to use and where to connect them. Typically, the more spider elements used, the better distribution of load and therefore better results. The connection locations of the spider elements to the full-featured geometry may also alter the accuracy of the model. The coupling of the connection between the 1D beam elements to the 3D featured model should be addressed to accurately represent the connection. A method proposed to understand the accurate representation is to analyze the model outside of a radius distance greater than the thickness of the featured connection location [39].

Spider geometry modeling for the wheel and hub model is shown in Fig. 4. The hub geometry is taken to be the same as the full-featured model. The wheel component is represented by spider elements. The adapter component is not modeled since it is no longer needed to

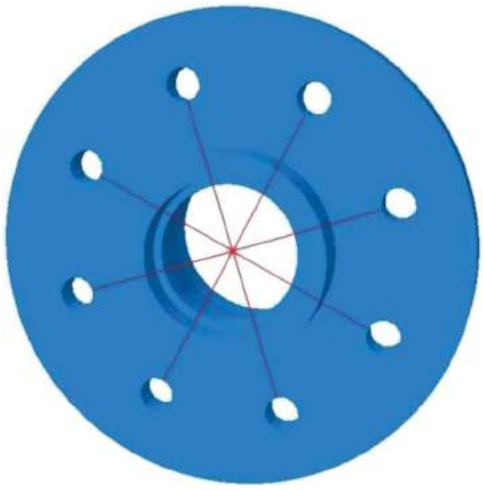

**Figure 4.** Spider modeling CAD geometry. Hub geometry is taken to remain the same, while the wheel is represented with spider elements. The adapter is removed, since it is no longer needed to apply the load.

**Figure 5.** CAD representation of shrinkwrapped wheel and featured hub geometry. Adapter component at the bottom of the wheel is incorporated for vertical load transfer.

apply loading to the model due to the load being applied at the center of the spider model. In the model shown, an eight-element model is used, with connections at each of the boltholes on the hub. Spider models with a variety of elements can be used, but the eight-element model is shown for demonstration purposes. The center point on the spider model is located where the center of mass of the wheel would be. The spider model represents the wheel in the assembly and transfers the load between the hub and the ground. This spider model is developed and analyzed manually in the finite element software.

## 6. Shrinkwrap geometry

We seek to improve on the performance of the previous geometry defeaturing methods. Defeaturing using the proposed shrinkwrap approach is discussed in this section. The proposed shrinkwrap geometry defeaturing approach is performed in the commercial CAD software PTC® Creo Parametric 2.0.

Though there are many levels of defeatured representations available in Creo Parametric 2.0, in this work we consider the standard defeatured level (level 1). We note that there are numerous levels of defeaturing that can be used, but we only focus on standard defeatured level in this study to show the applicability of the approach. Shrinkwrap is a feature in this software, which represents the exterior shape of the original source geometry with a collection of surfaces for an abstract representation. Typically, the shrinkwrap consists of reducing the complexity of the original geometry by enclosing holes and gaps, and removing any sharp edges and corners. The new shrinkwrap component can reduce the disk and memory usage significantly. For very intricate models, the geometry can be altered such that the volume and mass of the model change considerably. The shrinkwrap feature is able to assign the same mass properties to the new geometry that was in the original geometry (e.g., mass remains unchanged). Shrinkwrap modeling is able to represent complex assemblies with one, simple component or represent an individual component. Shrinkwrap modeling can also easily provide an accurate external representation of the model for use by other suppliers or customers without revealing the model's internal design. This feature is a benefit if others want to visualize the model for studies with their own work, while protecting trade secrets, patented designs, and other proprietary information.

The wheel and hub model with the full-featured hub and the shrinkwrapped, defeatured wheel is shown in Fig. 5. As in the previous defeaturing methods, we only defeature the wheel. The adapter component attached to bottom of the wheel is automatically modified to fit the geometry of the wheel. As shown in Fig. 5, the wheel is no longer represented with a circular outside diameter, but rather with numerous straight segments to create the outside diameter. The web of the wheel no longer has open holes and the transition from the web to the outside wheel surface is represented with a gradual slope rather than the sharp 90-degree angle in the full-featured geometry.

Using this shrinkwrap model, we are able to utilize the automated analysis process described in Section 2. The shrinkwrap process is performed in the preprocessing stage. The model runs through the same analysis process as in the full-featured geometry model.

## 7. Method and problem formulation

The proposed approach for shrinkwrap geometry defeaturing is implemented and analyzed using the automated system described in Section 2 for the wheel and hub model assembly presented in previous sections. Within the automated system, structural analysis is performed with the commercially available finite element-based CAE software, Dassault Systèmes Abaqus. The analysis is conducted for the shrinkwrap defeatured wheel and hub model, as well as a full-featured geometry, manual simplified geometry and spider model geometry to demonstrate the structural performance of the proposed approach.

The wheel and hub model is comprised of three components (hub, wheel and adapter) as described in Section 3. In all models analyzed, the hub is taken to have full-featured geometry. Geometry is defeatured on the wheel and adapter components.

The material of the hub, wheel and adapter are all taken to be stainless steel in this work. The Young's Modulus, Poisson's ratio and density are 197 GPa, 0.27 and 7.95 kg/m$^3$ respectively. The fatigue strength, yield strength, and ultimate tensile strength are 257.5 MPa, 205 MPa, and 515 MPa, respectively [25]. To simulate the location of restriction due to an axle, the inner radius of the hub is fixed in the x, y and z directions. Vertical gravity loads of 1 g are subjected for each of the components. A prescribed vertical load of 178 kN is distributed uniformly over the entire bottom surface of the adapter. The load is prescribed so that the maximum stress in the components would be near the fatigue strength of the material to provide a failure analysis.

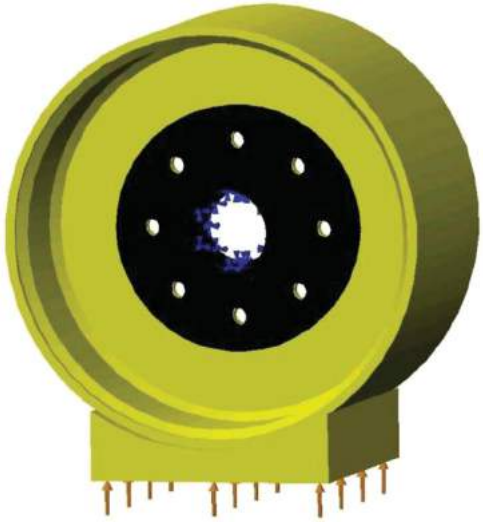

**Figure 6.** CAD model of wheel and hub featured geometry loading and boundary conditions. Blue triangles represent the fixed boundary conditions at the inside diameter of the hub. The arrows at the bottom of the adapter indicate the prescribed loading applied to the model. Gravity load not shown for vitalization purposes.

All examples considered in this work use the same dimensions, materials, boundary conditions and loading. The boundary conditions and loads are shown in Fig. 6. The geometry of the wheel is modified for the examples that utilize defeaturing. Each example uses the same finite element mesh parameters based on the model size, which restricts the mesh to a maximum element size based on the overall size of the component. The results of the finite element simulations and discussions for each geometry case are presented in the next section.

## 8. Results and discussion

In this section, we present results and discussion of a wheel and hub model prescribed with a vertical load to demonstrate the performance of the proposed shrinkwrap approach. The first example displays the behavior of the full-featured geometry wheel and hub model. The second example shows the response for manual simplified geometry of the full-featured wheel and hub. Results for spider geometry modeling of the wheel and hub are presented in the third example with three different spider representations. The fourth example covers the wheel and hub model for shrinkwrapped geometry. The discussion of all models considered in this section is summarized in the final subsection, Section 8.5.

### 8.1. Full-featured geometry results

In this work, the full-featured geometry is taken as the reference model. We compare the defeatured geometry models to the full-featured model to assess the accuracy. In this example, the hub, wheel and adapter have full-featured geometry based on the given CAD geometry. The model is meshed and analyzed using the automated system described in Section 2 for a finite element stress analysis of the hub. The mesh uses 51,873 total tetrahedral elements for the entire three-component assembly. Approximately 12,226 tetrahedral elements are used to model the hub. The finite element mesh is shown in Fig. 7.

The von Mises stress plot for the hub resulting from the prescribed loading is displayed in Fig. 8. The stress plots for the other components in the model are not shown since we are only concerned with the structural integrity of the hub. Similarly, for the remaining models analyzed in this section, only the hub results will be presented. Figure 8 shows the maximum stress (red) at the bottom of the inside diameter of the hub where the axle would connect to the hub. The maximum von Mises stress is predicted to be approximately 237.8 MPa. Due to the prescribed loading, the maximum stress occurs at

**Figure 7.** Finite element mesh for full-featured geometry wheel and hub model.

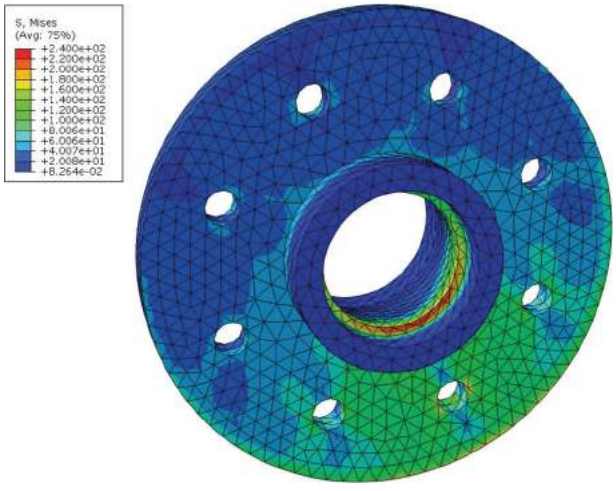


**Figure 8.** Hub stress plot for full-featured wheel and hub model.

the location where there is restriction of movement. The remainder of the hub displays much lower stress than the maximum stress with the majority of the top of the hub having minimal stress. Stress about half the magnitude of the maximum stress is shown adjacent to the maximum stress area around the inside diameter, as well as below the inside diameter in the bottom web.

### *8.2. Manual simplified geometry results*

In this example, we consider a wheel and hub model with manual simplified geometry for the wheel. The adapter geometry is the same as the full-featured geometry because the outer wheel geometry is not modified. For geometry defeaturing in this example, the full-featured geometry of the wheel is modified to enclose all holes.

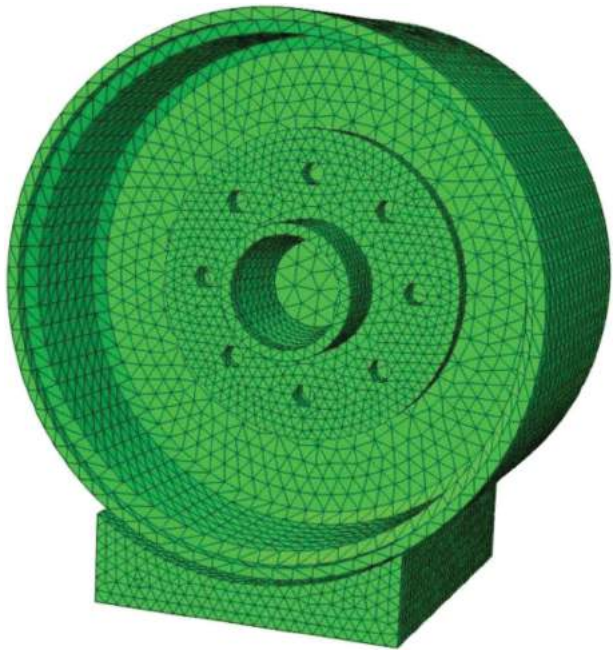

**Figure 9.** Finite element mesh for manual simplified geometry wheel and hub model.

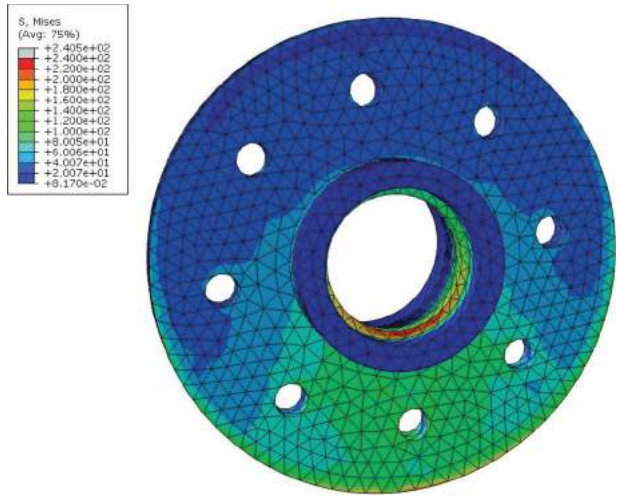


**Figure 10.** Hub stress plot for manual simplified geometry wheel and hub model. Plot is normalized with the full-featured plot for comparison.

The enclosure of holes in the wheel creates a geometry that is easier to mesh and analyze. The CAD component for the wheel is manually modified prior to using the automated analysis process. 51,000 total tetrahedral elements are used to mesh the entire three-component assembly. The finite element mesh is shown in Fig. 9.

Figure 10 shows the von Mises stress plot on the hub due to the prescribed loading. For visualization and comparison purposes, the magnitude of the plot is normalized with that of the full-featured geometry hub stress

plot. Any stress above 240 MPa is indicated by grey on the plot. For this case of defeatured geometry, the maximum stress is 240.5 MPa and is approximately at the same location of the bottom of the inside diameter of the hub. Similar to the full-featured geometry, minimal stress is displayed at the top of the hub web and larger stress is located at the inside diameter of the hub as well as the bottom of the web. A location of near maximum stress is also located at the bottom of the hub.

### 8.3. Spider geometry modeling results

This example covers the spider modeling geometry to defeature the wheel and hub model. The same full-featured geometry is used for the hub as in the previous examples. The wheel is defeatured with spider elements. The adapter is not modeled in this example because the vertical load is now applied at the center of the spider elements. Spider modeling involves connecting the spider elements (beam elements) directly to finite element nodes on the hub mesh. The finite element mesh for the hub uses 12,226 tetrahedral elements. We consider three different spider model configurations in this section to access variations of spider modeling.

The spider model configurations consist of rigid 1D beam elements connected at one central point, the wheel center of mass. Each of the rigid beam elements are equal in length and are unable to deform. The ends of each beam element connect to a node at a bolthole location. They are placed accordingly to distribute the prescribed loading on the hub. The center point of the spider model has a point mass associated with the total mass of the featured wheel. The center point is loaded with a 178 kN vertical load and 1 g gravity load. The centrally applied load represents the same load as the full-featured geometry model.

The first spider model example utilizes eight rigid elements or "legs". Each leg is attached to the inside of each of the boltholes on the hub at the center of the thickness of the hole. The finite element mesh of the eight-leg hub model is represented in Fig. 11. The red lines represent each of the legs.

Figure 12 shows the von Mises stress plot on the hub for the eight-leg spider model. The plot is normalized in magnitude from the stress hub plot for full-featured geometry example for comparison. The eight-leg spider model produces multiple locations of singularities around the boltholes of the hub from the connection of the spider legs to each hole. The stress appears to be minimal on the outside web of the hub and with slightly larger stress in the web adjacent to the inside diameter of the hub. The stress singularities are common in spider modeling from the leg to node connections due to the mixed

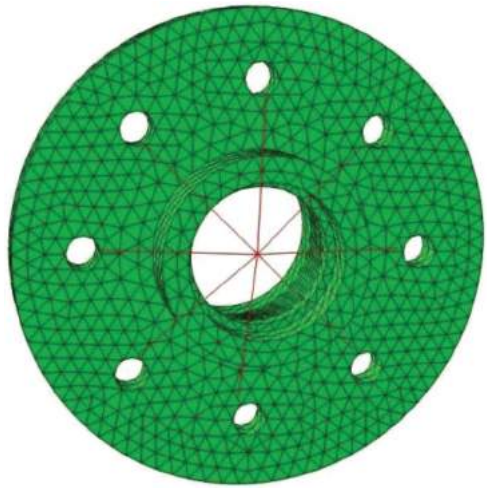

**Figure 11.** Finite element mesh for eight-leg spider wheel and hub model. Hub is modeled with full-featured geometry and the wheel is modeled with spider elements. Each bolthole connects one spider leg.

dimensional modeling. Due to this phenomenon, it is common practice to disregard a certain distance around the spider leg connection location. In this work, based on the model size and finite element mesh, we disregarded approximately the radius of the hub thickness at the location of the multidimensional (1D-3D) element connection. Applying this distance to the model, the entire web of the hub is disregarded and we only consider the center of the hub to contain valid stress results. With this in mind, the location of maximum stress is estimated at the inside diameter of the hub. The maximum stress is found to be approximately 114 MPa.

We can try to alleviate the amount of singularities in the spider model by applying additional spider legs to model the wheel. We consider 32 total spider legs, where four legs are attached to each bolthole at the center thickness of the web. The finite element mesh for the 32-spider leg example is shown in Fig. 13. The red lines represent each of the legs.

Analysis of the 32-leg spider model results in the von Mises stress hub plot displayed in Fig. 14. The plot is normalized in magnitude from the stress hub plot for full-featured geometry example for comparison. Singularities arise in the 32-leg spider model at the location of the spider leg to node connections by the boltholes, similar to that of the eight-leg spider model. However, it appears that there is a reduction in the amount of singularities compared to the eight-leg model. Similar to the eight-leg spider model, we must disregard a distance around the spider leg to node connections. The same distance to disregard the stress is taken in this model (e.g., thickness of the location of the connection which leads to consider

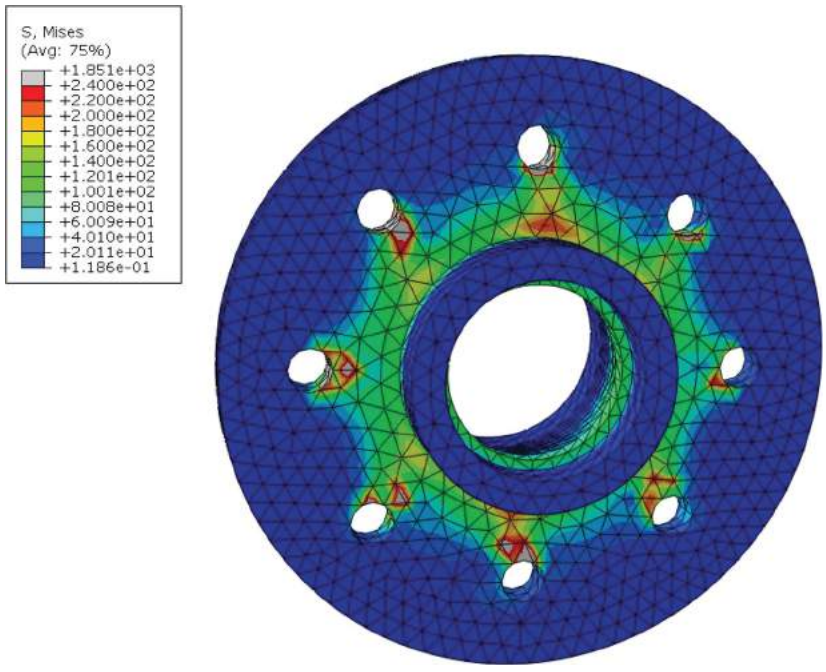


**Figure 12.** Hub stress plot for eight-leg spider model. Plot is normalized with the full-featured plot for comparison.

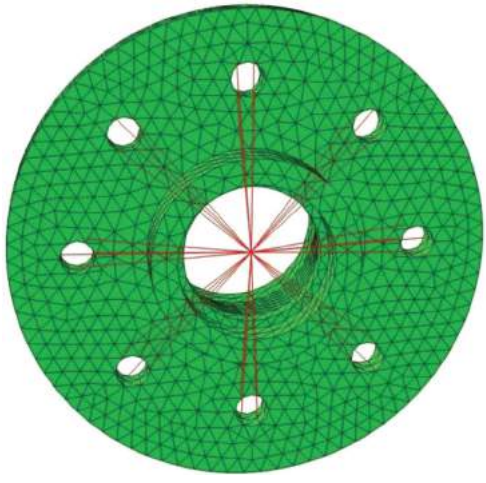

**Figure 13.** Finite element mesh for 32-leg spider wheel and hub model. Hub is modeled with full-featured geometry and the wheel is modeled with spider elements. Each bolthole connects four spider legs.

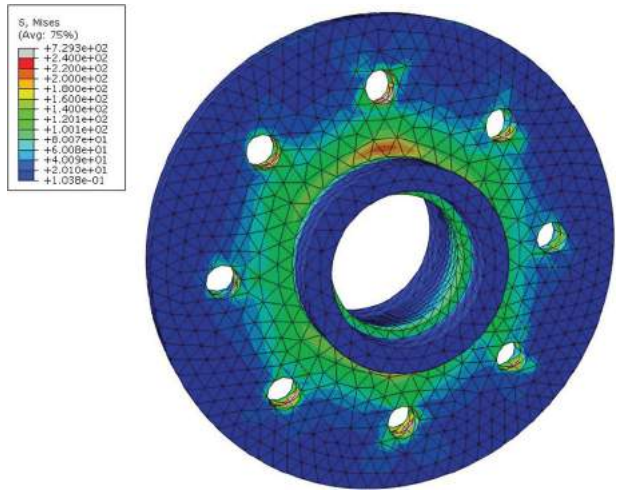


**Figure 14.** Hub stress plot for 32-leg spider model. Plot is normalized with the full-featured plot for comparison.

only the center of the hub for valid stress results). The maximum stress is approximately 115 MPa at the inside diameter of the hub.

The spider model is modified again, with 96 total legs to give a more accurate representation of the wheel and hub. Twelve legs are attached to nodes at each bolthole location for the transfer of the load. The finite element mesh for the 96-spider leg example is shown in Fig. 15. The red lines represent each of the legs.

Figure 16 shows the von Mises stress plot of the hub for the 96-leg spider model. The plot is normalized in magnitude from the stress hub plot for full-featured geometry example for comparison. The 96-leg model yields singularities similarly to that of the previous spider model examples, therefore we apply the same distance to disregard in the stress plot to accurately assess the model. With only the center of the hub of model remaining to analyze, the inside diameter of the hub displays the largest stress. The maximum stress in the model is approximately 120 MPa.

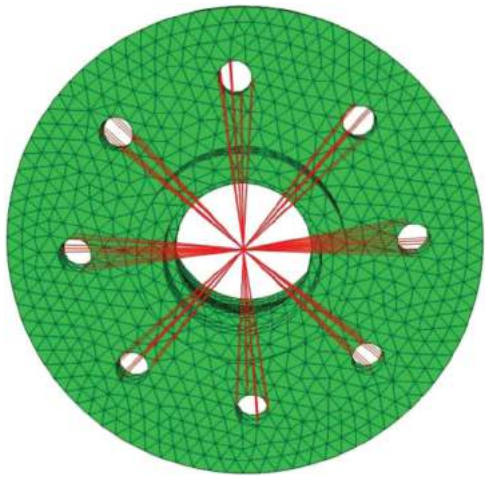

**Figure 15.** Finite element mesh for 96-leg spider wheel and hub model. The hub is modeled with full-featured geometry and the wheel is modeled with spider elements. Each bolthole connects 12 spider legs.

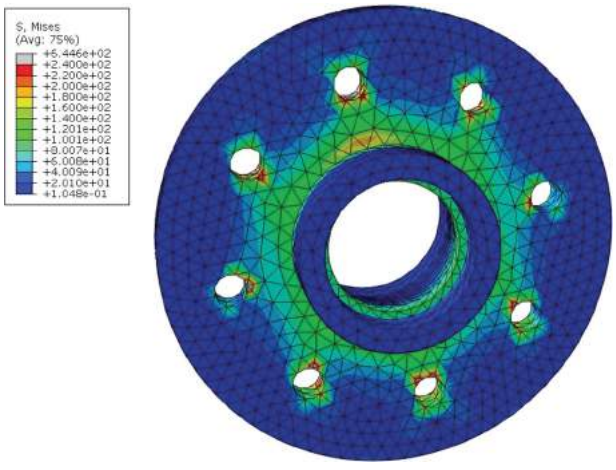


**Figure 16.** Hub stress plot for 96-leg spider model. Plot is normalized with the full-featured plot for comparison.

### 8.4. Shrinkwrap geometry results

The proposed shrinkwrap defeaturing approach is investigated in this example. As in the previous examples, the hub geometry is modeled with the full-featured CAD model. The wheel is defeatured with the proposed shrinkwrap approach. The adapter is modified to fit the dimensions of the defeatured wheel. When preprocessing the CAD model, the shrinkwrap defeaturing of the wheel is performed with the first level of simplification. The defeaturing of the shrinkwrap approach removes all the holes and sharp edges on the component. The finite element mesh used in the analysis is displayed in Fig. 17. The mesh consists of a total of 62,294 tetrahedral elements, which is more than the full-featured model. The mesh is not optimized in the shrinkwrap model and uses

**Figure 17.** Finite element mesh for shrinkwrap geometry wheel and hub model.

the same mesh parameters as the other models, resulting in an increase in elements.

The von Mises stress hub plot for the shrinkwrap defeatured geometry wheel hub model is displayed in Fig. 18. The plot is normalized in magnitude from the stress hub plot for full-featured geometry example for comparison.

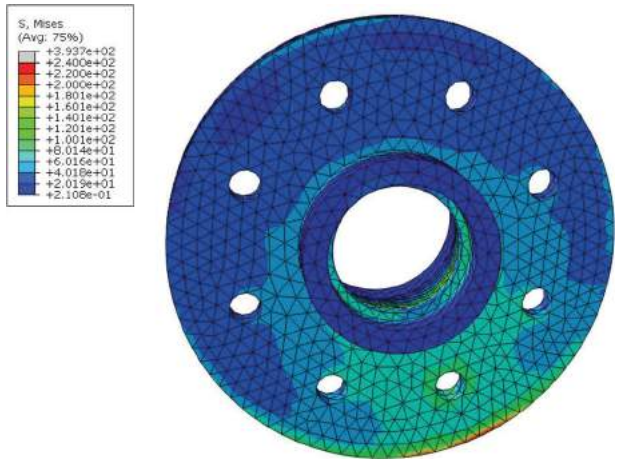


**Figure 18.** Hub stress plot for wheel and hub shrinkwrap geometry model. Plot is normalized with the full-featured plot for comparison.

The maximum stress is located at the bottom of the inside diameter of the hub. At this location, two singularities develop as shown in Fig. 19. The singularities are removed from the analysis of the stress plot because they result in a rapid stress gradient at the associated node due to the change in geometry of the wheel. Once the singularities are removed, the maximum stress is located in the

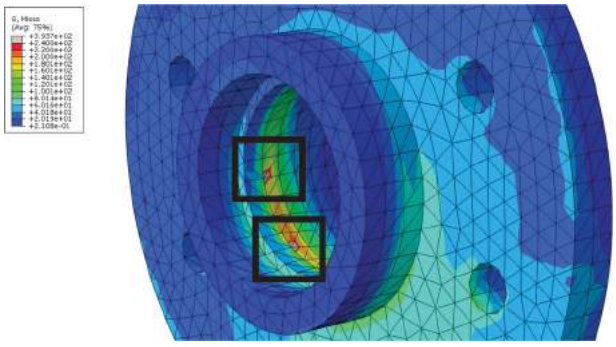

**Figure 19.** Resultant singularities from the defeatured shrinkwrap geometry of the wheel. Two locations of singularities are present at the inside diameter of the hub, noted with boxes.

same area as with the other methods considered, located at the bottom of inside diameter of the hub. The maximum stress is approximately 240 MPa. Minimal stress is observed at the top web of the hub and larger stress located at the bottom of the web and at the inside diameter of the hub. A location of near maximum stress is located at the bottom of the hub, which is similar to the full-featured results.

### 8.5. Results summary

The wheel and hub model is structurally analyzed for geometry defeaturing of the wheel in three different methods: manual simplified geometry, spider modeling, and shrinkwrap defeatured geometry. The defeatured models are compared with the full-featured geometry model for reference.

The full-featured geometry hub stress plot displays maximum stresses around the inside diameter of the hub, and has minimal stress at the top of the hub with larger stress values at the bottom of the hub.

The maximum stresses estimated in the manual simplified geometry model are located around the inside diameter of the hub, similarly to that of the full-featured model. The overall stress distribution is found to be very similar to that of the full-featured model with deviation around the boltholes, which is appropriate because of the minor change in geometry of the wheel at the holes.

Spider models using 8, 32, and 96 legs are considered in this analysis. As we increase the amount of the spider legs used in the model, the size and amount of the singularities decrease because of the increase of load distribution. Since the legs of the spider model transfer load to a particular node on the finite element mesh, singularities are produced and stress distributions around the leg connection locations must be ignored to accurately distinguish the behavior of the hub. For all three spider model cases, therefore the maximum stresses are located around the inside diameter of the hub, with the 96-leg spider model having the largest stress closest to the full-featured model. We also note that the stress distributions on the hub do not follow the same pattern as the full-featured model.

The shrinkwrap model maximum stress is located around the inside diameter of the hub, similar to the full-featured model. The stress distribution on the hub of the shrinkwrap model is also similar to that of the full-featured model. The proposed shrinkwrap approach results in singularities at the inside diameter of the hub. In our interpretation of the results, we excluded stress singularities when considering maximum von Mises stress. A summary of the maximum von Mises stresses for all models considered is located in Fig. 20.

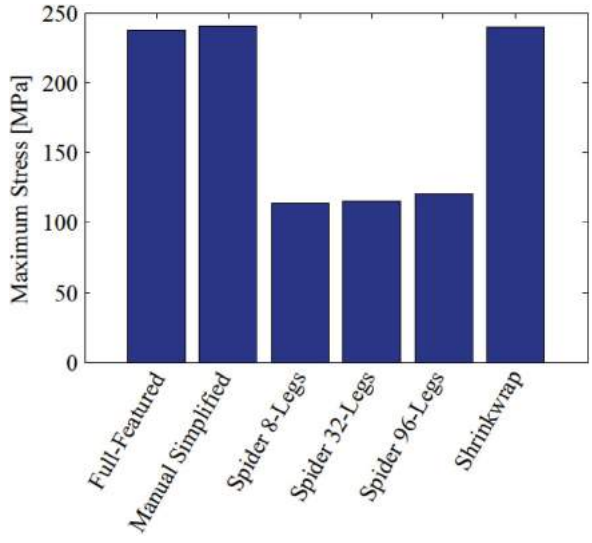


**Figure 20.** Maximum summary stresses for featured and defeatured geometry models. The absolute errors of the maximum stresses as compared with the full featured model are approximated as 0.9% for the shrinkwrap approach, 1.1% for the manual simplified geometry and 52%, 51% and 49% for the 8, 32, and 96 leg spider models respectively. Maximum stresses do not include singularities and the spider models did not consider the area around the spider connections.

Each of the defeatured models that are considered provides benefits and disadvantages in the modeling process. The manual simplified geometry provides accurate representation compared to the featured model, but the geometry had to be modified manually (yielding an approximate error of 1.1%), slowing down the analysis process and retains much of the complex geometry of the full-featured model. Modifying components using the manual modified geometry on a larger model would not be efficient for preprocessing in the analysis. The computational time to complete the structural analysis for the

**Table 1.** Summary of methods use to model wheel and hub assembly. All methods used the same element parameters in the mesh (e.g., max size, min size).

| Processing Model | Mesh Elements | Volume ($cm^3$) | Singularities |
|---|---|---|---|
| Full-Featured | 51,873 | 3,800 | No |
| Manual simplified | 51,000 | 3,820 | No |
| 8 leg spider | 12,234 | 379 | Yes |
| 32 leg spider | 12,258 | 379 | Yes |
| 96 leg spider | 12,322 | 379 | Yes |
| Shrinkwrap | 62,294 | 5,633 | Yes |

spider modeling was the fastest of the models considered. This reduction in computational time is due to the significant reduction in the volume and amount of finite elements used in the model. However, the spider modeling provides numerous singularities requiring expert analysis of the results. When increasing the number of spider legs used, the number of singularities decrease. For all three spider models considered, we manually inspect each model to understand the behavior of the hub. After disregarding the locations of irrelevant stress, the maximum stress is approximately half the maximum stress of the full-featured geometry (i.e. 49–51% approximate absolute error). For all spider model cases, the spider legs are created manually in the finite element software, which is not an efficient task. In general, the spider modeling provides a quick processing analysis yet significant preprocessing time.

The proposed shrinkwrap approach provides results similar to the full-featured model. The maximum stress for the shrinkwrap model has an approximate absolute error of 0.9% compared to the featured model, even though the volume of the shrinkwrap model is approximately 1.5 times larger than the full-featured model. The larger volume results in an increase in the amount of elements due to the maximum elements size limit that was held constant for all simulations. Although the proposed shrinkwrap approach creates singularities, the number of singularities is minimal. The automated process is easily used with the shrinkwrap approach, resulting in the same preprocessing time as the full-featured model. Overall, the proposed shrinkwrap approach provides a reasonable method to estimate the structural performance of the model for defeatured geometry of the components that are not assessed for their structural integrity but are able to transfer loads, and is in better agreement than the spider modeling. A summary of the geometry models analyzed with the number of mesh elements, volume and singularities is located in Table 1.

## 9. Conclusions

We propose an automated approach to accurately estimate the structural performance for component design using the shrinkwrap defeatured geometry for components that are not assessed for their structural integrity. Defeatured shrinkwrap modeling is performed in PTC® Creo Parametric 2.0 and utilizes an automated system to structural analyze the model using FEA. We review manual simplified geometry, spider modeling and the proposed shrinkwrap defeaturing approach and assess them with the full-featured geometry of a hub and wheel model. The shrinkwrap defeaturing approach is found to provide an accurate estimation on the structural performance compared to the full-featured geometry model and is more accurate than the spider abstraction model.

Future work remains on this topic. We reviewed the behavior of a small component (hub) of an assembly (wheel and hub) in this manuscript. Next, we will look into different, larger, and more complex models and their specific components that can be addressed with shrinkwrap approach. Models that are complex and models that may not be able to be meshed adequately could possibly benefit significantly from the shrinkwrap approach. The various levels of defeaturing in the shrinkwrap process will also be performed to investigate the response for the different geometry abstractions. A mesh sensitivity study will also need to be conducted on the wheel and hub model as well as additional models to understand the effect of the initial mesh size on each of the components and for re-meshing the components to optimize performance. While the current study resulted in more elements for the shrinkwrap approach, we anticipate mesh optimization will produce favorable results, both in computational resources and total analysis time. Shrinkwrap modeling using the in-house tool suite for performing accurate thermal analysis can also be assessed. Singularities arose in both the shrinkwrap and spider defeatured models and an investigation into the singularities will be performed, including the effect from mesh parameters and defeaturing level. We are also interested in developing automated processes to characterize, assess and disregard singularities in the structural analysis of models, with the goal of providing an automated way of analyzing assemblies while achieving accurate results.

## Acknowledgements

The authors would like to acknowledge the financial support from the Defense Advanced Research Projects Agency (DARPA) under contract HR0011-13-C-0041.

## ORCID

*Matthew G. Pike* http://orcid.org/0000-0002-7448-7515
*Michael R. Myers* http://orcid.org/0000-0002-7732-3997

## References


[1] Aguirrebeitia, J.; Abasolo, M.; Aviles, R.; Fernandez de Bustos. I.: General static load carrying capacity for the design and selection off our contact point slewing bearings: finite element calculations and theoretical model validation, Finite Elements in Analysis and Design, 55, 2012, 23–30. http://dx.doi.org/10.1016/j.finel.2012.02.002

[2] Balmelli, L.; Vetterli, M.; and Liebling, T. M.: Mesh optimization using global error with application to geometry simplification, Graphical Models, 64(3), 2002, 230–257. http://dx.doi.org/10.1016/0020_7683(73)90082-6

[3] Beall, M. W.; Walsh, J.; Shephard, M. S.: Accessing CAD Geometry for Mesh Generation, In IMR, 2003, pages 33–42.

[4] Bellenger, E.; Coorevits, P.: New approach for automation of finite element analysis, Journal of Computational and Applied Mathematics, 168(1), 2004, 65–75. http://dx.doi.org/10.1016/j.cam.2003.05.011

[5] Chahine, E.; Laborde, P.; Renard, Y.: Spider XFEM, an extended finite element variant for partially unknown crack-tip displacement, European Journal of Computational Mechanics, 17(5–7), 2008, 625–636. http://dx.doi.org/10.3166/REMN.17.625-636

[6] De Martino, T.; Falcidieno, B.; and Haßinger, S.: Design and engineering process integration through a multiple view intermediate modeller in a distributed object-oriented system environment, Computer-Aided Design, 30(6), 1998, 437–452. http://dx.doi.org/10.1016/S0010-4485(97)00096-1

[7] Dey, S.; Shephard, M. S.; Georges, M. K.: Elimination of the adverse effects of small model features by the local modification of automatically generated meshes, Engineering with Computers, 13(3), 1997, 134–152. http://dx.doi.org/10.1007/BF01221211

[8] Dos Santos, C. H.; Bittencourt, G.; Guenther, R.; De Pieri, E.: A fuzzy hybrid singularity avoidance for underwater vehicle-manipulator systems, In 12th IFAC Symposium on Information Control Problem in Manufacturing, 2006.

[9] Fine, L.; Remondini, L.; Leon, J.-C.: Automated generation of FEA models through idealization operators, International Journal for Numerical Methods in Engineering, (1–2), 2000, 83–108.

[10] Finnigan, P.; Kela, A.; Davis, J.: Geometry as a basis for finite element automation, Engineering with Computers, 5(3–4), 1989, 147–160. http://dx.doi.org/10.1007/BF02274209

[11] Foucault, G.; Cuillière, J.-C.; François, V.; Lèon, J.-C.; Maranzana, R.: Adaptation of CAD model topology for finite element analysis, Computer-Aided Design, 40(2), 2008, 176–196. http://dx.doi.org/10.1016/j.cad.2007.10.009

[12] Foucault, G.; Marin, P. M.; Lèon, J.-C.: Mechanical criteria for the preparation of finite element models, In IMR, 2004, pages 413–426.

[13] Gopalakrishnan, S. H.; Suresh, K.: A formal theory for estimating defeaturing-induced engineering analysis errors, Computer-Aided Design, 39(1), 2007, 60–68. http://dx.doi.org/10.1016/j.cad.2006.09.006

[14] GrabCad: Forklift, lift truck r2, 2001, https://grabcad.com/library/forklift-lift-truck-r2

[15] Institute for Software Integrated Systems: META tool suite, 2014. http://www.isis.vanderbilt.edu

[16] Kim, J.; Yoon, J.-C.; Kang, B.-S.: Finite element analysis and modeling of structure with bolted joints, Applied Mathematical Modelling, 31(5), 2007, 895–911. http://dx.doi.org/10.1016/j.apm.2006.03.020

[17] Leclerc, W.; Karamian-Surville, P.; Vivet, A.: An efficient and automated 3D FE approach to evaluate effective elastic properties of overlapping random fibre composites, Computational Materials Science, 99, 2015, 1–15. http://dx.doi.org/10.1016/j.commatsci.2014.10.047

[18] Lee, S. H.: A CAD-CAE integration approach using feature-based multi-resolution and multi-abstraction modelling techniques, Computer-Aided Design, 37(9), 2005, 941–955. http://dx.doi.org/10.1016/j.cad.2004.09.021

[19] Li, M.; Gao, S.: Estimating defeaturing-induced engineering analysis errors for arbitrary 3D features Computer-Aided Design, 43(12), 2011, 1587–1597. http://dx.doi.org/10.1016/j.cad.2011.08.006

[20] Li, M.; Gao, S.; Martin, R. R.: Estimating the effects of removing negative features on engineering analysis, Computer-Aided Design, 43(11), 2011, 1402–1412. http://dx.doi.org/10.1016/j.cad.2011.08.013

[21] Li, M.; Gao, S.; Martin, R. R.: Engineering analysis error estimation when removing finite-sized features in nonlinear elliptic problems, Computer-Aided Design, 45(2), 2013, 361–372. http://dx.doi.org/10.1016/j.cad.2012.10.019

[22] Li, M.; Gao, S.; Zhang, K.: A goal-oriented error estimator for the analysis of simplified designs, Computer Methods in Applied Mechanics and Engineering, 255, 2013, 89–103. http://dx.doi.org/10.1016/j.cma.2012.11.010

[23] Li, Z.-C.: The schwarz alternating method for singularity problems, SIAM Journal on Scientific Computing, 15(5), 1994, 1064–1082. http://dx.doi.org/10.1137/0915065

[24] Malone, J. G.; Hodge, P. G.; Plunkett, R.: Finite element mesh for a complete solution of a problem with a singularity, Computers & Structures, 24(4), 1986, 613–623. http://dx.doi.org/10.1016/0045-7949(86)90200-2

[25] MatWeb, LLC: Material property data, 2015, http://www.matweb.com

[26] McCune, R.; Armstrong, C.; Robinson, D.: Mixed-dimensional coupling in finite element models, International Journal for Numerical Methods in Engineering, 49(6), 2000, 725–750. http://dx.doi.org/10.1002/1097-0207(20001030)49:6 < 725::AID-NME967 > 3.0.CO;2-W

[27] Mobley, A. V.; Carroll, M. P.; Canann, S. A.: An object oriented approach to geometry defeaturing for finite element meshing, In IMR, 1998, pages 547–563.

[28] Montgomery, J.: Methods for modeling bolts in the bolted joint, In ANSYS User's Conference, volume 5, 2002.

[29] Moon, H.; Lee, M.; Joun, M.: An approximate efficient finite element approach to simulating a rotary forming process and its application to a wheel-bearing assembly, Finite Elements in Analysis and Design, 44(1), 2007, 17–23. http://dx.doi.org/10.1016/j.finel.2007.08.003

[30] Nam, C.; Lee, M.; Eom, J.; Choi, M.; Joun, M.: Finite element analysis model of rotary forging for assembling wheel hub bearing assembly, Procedia Engineering, 81, 2014, 2475–2480.

[31] Philbrick, G.; Rietz, R.: High-fidelity modeling of an aerospace structure comprised of bolted joints, In Proceedings of SEM, 2006.
[32] Pin, T.; Pian, T. H.: On the convergence of the finite element method for problems with singularity, International Journal of Solids and Structures, 9(3). 1973, 313–321. http://dx.doi.org/10.1016/0020-7683(73)90082-6
[33] Purohit, R.; Khitoliya, P.; Koli, D. K.: Design and finite element analysis of an automotive clutch assembly, Procedia Materials Science, 6, 2014, 490–502.
[34] Quadros, W. R.; Owen, S. J.: Defeaturing CAD models using a geometry-based size field and facet-based reduction operators, Engineering with Computers, 28(3), 2012, 211–224. http://dx.doi.org/10.1007/s00366-011-0252-8
[35] Ramabathiran, A.; Gopalakrishnan, S.: Automatic finite element formulation and assembly of hyperelastic higher order structural models, Applied Mathematical Modelling, 38(11), 2014, 2867–2883. http://dx.doi.org/10.1016/j.apm.2013.11.021
[36] Ramanan, L.; Kumar, R. K.; Sriraman, R.: Thermomechanical finite element analysis of a rail wheel, International Journal of Mechanical Sciences, 41(4), 1999, 487–505.
[37] Sanayei, M.; Rohela, P.: Automated finite element model updating of full-scale structures with PARameter Identification System (PARIS), Advances in Engineering Software, 67, 2014, 99–110. http://dx.doi.org/10.1016/j.advengsoft.2013.09.002
[38] Shephard, M. S.: Finite element modeling within an integrated geometric modeling environment: Part II Attribute specification, domain differences, and indirect element types, Engineering with Computers, 1(2), 1985, 73–85.
[39] Shim, K. W.; Monaghan, D. J.; Armstrong, C. G.: Mixed dimensional coupling in finite element stress analysis, Engineering with Computers, 18(3), 2002, 241–252. http://dx.doi.org/10.1007/s003660200021
[40] Siddiqui, N. A.; Khan, M. Z.; Munir, A.; Deen, K.; Amin, M. A.: Failure investigation of wheel gear hub assembly of an aircraft, Engineering Failure Analysis, 22, 2012, 73–82. http://dx.doi.org/10.1016/j.engfailanal.2012.01.004
[41] Simpson, R.: Enrichment of the boundary element method through the partition of unity method for fracture analysis using local and global formulations, Ph.D. thesis, Durham University (2010).
[42] Staab, G.: Estimating singularity powers with finite elements, Computers & Structures, 17(1), 1983, 73–78. http://dx.doi.org/10.1016/0045-7949(83)90031-7
[43] Stolk, J.; Verdonschot, N.; Mann, K.; Huiskes, R.: Prevention of mesh-dependent damage growth in finite element simulations of crack formation in acrylic bone cement, Journal of Biomechanics, 36(6), 2003, 861–871. http://dx.doi.org/10.1016/S0021-9290(03)00003-4
[44] Szabo, B. A.; Babuska, I.: Finite element analysis, John Wiley & Sons, 1991.
[45] Sze, K.; Wang, H.-T.: A simple finite element formulation for computing stress singularities at bimaterial interfaces, Finite Elements in Analysis and Design, 35(2), 2000, 97–118. http://dx.doi.org/10.1016/S0168-874X(99)00057-8
[46] Tautges, T. J.: Automatic detail reduction for mesh generation applications, In Proceedings 10th International Meshing Roundtable, 2001, pages 407–418.
[47] Tennyson, J.; Sutcliffe, B. T.: Dicretization to avoid singularities in vibration–rotation Hamiltonians: A bisector embedding for AB2 triatomics, International Journal of Quantum Chemistry, 42(4), 1992, 941–952.
[48] Tekkaya, A.: Martins, P.: Accuracy, reliability and validity of finite element analysis in metal forming: a user's perspective, Engineering Computations, 26, 2009, 1026–1055.
[49] Thakur, A.; Banerjee, A. G.; Gupta, S. K.: A survey of CAD model simplification techniques for physics-based simulation applications, Computer-Aided Design, 41(2), 2009, 65–80. http://dx.doi.org/10.1016/j.cad.2008.11.009
[50] Truman, C.; Booker, J.: Analysis of a shrink-fit failure on a gear hub/shaft assembly, Engineering Failure Analysis, 14(4), 2007, 557–572. http://dx.doi.org/10.1016/j.engfailanal.2006.03.008
[51] Turevsky, I.; Gopalakrishnan, S. H.; Suresh, K.: Defeaturing: a posteriori error analysis via feature sensitivity, International Journal for Numerical Methods in Engineering, 76(9), 2008, 1379–1401. http://dx.doi.org/10.1002/nme.2345
[52] Volpin, O.; Sheffer, A.; Bercovier, M.; Joskowicz, L.: Mesh simplification with smooth surface reconstruction, Computer-Aided Design, 30(11), 1998, 875–882. http://dx.doi.org/10.1016/S0010-4485(98)00044-X
[53] Weißgraeber, P.; Becker, W.: Crack Initiation at Weak Stress Singularities-Finite Fracture Mechanics Approach, Procedia Materials Science, 3, 2014, 153–158.
[54] Williamson, S.; Gersh, D.: Representation of rotor spiders in reduced finite-element models for cage rotors, In Electrical Machines and Drives, 1995, pages 72–76. IEE. http://dx.doi.org/10.1049/cp:19950838
[55] Winter, O.; Ucsnik, S.; Rudolph, M.; Kral, C.; Schmidt, E.: Ironless in-wheel hub motor design by using multi-domain finite element analyses, In Power Electronics, Electrical Drives, Automation and Motion (SPEEDAM), 2012 International Symposium on, 2012, pages 1474–1478. IEEE. http://dx.doi.org/10.1109/SPEEDAM.2012.6264394